RSC Advances

PAPER

View Article Online
View Journal | View Issue

Cite this: *RSC Adv.*, 2020, **10**, 3726

Reversible photo-responsive gel–sol transitions of robust organogels based on an azobenzene-containing main-chain liquid crystalline polymer†

Jing Wang,[a] Qian Jiang,[a] Xingtian Hao,[a] Hongchao Yan,[a] Haiyan Peng,[a] Bijin Xiong,[a] Yonggui Liao *[ab] and Xiaolin Xie[ab]

Received 4th December 2019
Accepted 7th January 2020

DOI: 10.1039/c9ra10161f

rsc.li/rsc-advances

Stimuli-responsive supramolecular gels have been widely investigated, but the construction of a liquid crystalline gel with a high mechanical property and reversible photo-response still remains a challenge. This is due to the difficulty of designing gelators with liquid crystal properties and gelation abilities in organic solvents simultaneously. In this study, an azobenzene-containing main-chain polyester (Azo-mLCP) with a pendant amide group was synthesized. The organogel of Azo-mLCP *via* a hydrogen bond in dioxane possessed reversible thermal- and photo-responsive behaviours. The organogel exhibited a good self-supporting ability when the concentration of the gelator was more than 7.5 wt%. The rapid *trans*-to-*cis* isomerization of Azo-mLCP in solution was studied *via* UV-Vis absorption spectra. In addition, the gel-to-sol transition of the organogel could be triggered efficiently by an incomplete *trans*-to-*cis* conversion strategy. This study opens a way for the main-chain liquid crystalline polymers to serve in potential applications in photo-responsive robust actuators, electro-optical devices, and so on.

Introduction

A stimuli-responsive supramolecular gel is a kind of interesting material that can respond to external stimuli, such as temperature, light, pH and magnetic fields.[1,2] Among these triggers, light has attracted considerable interest as it is can be localized in space and precisely controlled without a direct contact.[3,4] Moreover, the photochemical processes do not require extra additives, and by-products are limited in most cases. Traditionally, a certain class of photochromic compounds, such as azobenzene, spiropyran[5] and diarylethene,[6] can be covalently conjugated with non-photoresponsive building blocks to achieve photo-tunable molecular assemblies.[7] The photo-induced and thermal geometric isomerization of azobenzene, a wonderful photo-responsive group, has been extensively studied over the last four decades.[8] The key attractive feature is the unique reversible *trans–cis–trans* isomerization cycles upon exposure to UV and visible lights. The configuration changes accompanied with photo-isomerization are capable of tailoring the chemical and physical properties, which allow the applications of photo-responsive supramolecular organogels in drug deliveries, soft actuators, optical devices, self-healing materials, *etc.* A self-healing organogel of azobenzene-grafted poly(carboxylic acid) in DMF driven by hydrogen bonds and cation–π interactions has been achieved.[9] Besides, a photo-responsive dextran hydrogel constructed *via* the host–guest interactions between *trans*-azo and cyclodextrin in the pendent polymer chains has been employed for light-controlled protein release.[10] In addition, a gel from poly(amide-triazole) bearing azobenzene units along the main chain has a reversible gel–sol transformation, which can be smoothly triggered by UV and visible light irradiation, but the gel is soft with a saturated storage modulus of less than 10^3 Pa.[11]

In recent years, azobenzene-containing liquid crystalline polymers (LCPs) have drawn considerable attention because they combine the intriguing photo-responsive property and anisotropic liquid crystalline behaviours related to the rod-like *trans*-azo mesogens.[12–14] So far, a great number of LCPs with azobenzene mesogens have been reported. The mechanical properties and photo-responses of azobenzene LCPs are strongly related to the position of the azobenzene group, *i.e.* whether in the main chain or in the side chain.[15] The azobenzene-containing main-chain LCPs, in comparison with the side chain ones, display more prominent mechanical properties and more efficient *trans*-to-*cis* isomerization. A nematic monodomain liquid crystalline elastomer (LCE) based on mixed main- and side-chains showed that the elongation

[a]*Key Laboratory of Material Chemistry for Energy Conversion and Storage, Ministry of Education, Hubei Key Laboratory of Material Chemistry and Service Failure, School of Chemistry and Chemical Engineering, Huazhong University of Science and Technology, Wuhan 430074, China. E-mail: ygliao@mail.hust.edu.cn*

[b]*National Anti-counterfeit Engineering Research Center, Huazhong University of Science and Technology, Wuhan 430074, China*

† Electronic supplementary information (ESI) available: The α, β and π^* values for different solvents; summary of the K_{tc}, t_∞ and P of UV light irradiation; ^{1}H NMR spectra of Azo-mLCP in d_8-dioxane at different concentrations; POM images of Azo-mLCP organogel before and after UV light irradiation. See DOI: 10.1039/c9ra10161f

increased with the proportion of the main-chain component *versus* the side chain one.[16] Azobenzene-containing main-chain LCPs displayed a huge response due to the prominent backbone anisotropy and large coupling constant to the underlying order parameter.[15]

Although the gels based on photo-responsive main-chain LCPs are expected to possess high mechanical properties and efficient photo-isomerization behaviours, the design and synthesis of such a polymeric gelator with liquid crystal properties and gelation abilities is still a formidable challenge. Herein, we synthesized a novel kind of azobenzene-containing main-chain liquid crystalline polyester with a pendent amide group, which could self-assemble into an organogel in dioxane by hydrogen bonds and π–π interactions. In addition, the organogel displayed a self-supporting behaviour, which was attributed to the excellent mechanical property of the main-chain LCP gelator. Finally, the efficient gel–sol transition could be achieved by the incomplete *trans*-to-*cis* conversion strategy upon UV light irradiation. Based on these characteristics, many potential applications can be proposed for this kind of organogel, such as soft actuators, molecular switches and photomechanical systems.[12,17–20]

Experimental

Materials

4-Aminophenol was obtained from Alfa Aesar Co., Inc. 4,4′-Biphenol, 2-(2-(2-chloroethoxy)ethoxy)ethanol, diethyl acetamidomalonate, potassium iodide (KI) and tetrabutyl orthotitanate ($Ti(O^iPr)_4$) were supplied by TCI Development Co., Ltd. Ethyleneglycol dimethyl ether was supplied by Aladdin Bio-Chem Technology Co., Ltd. Sodium nitrite (Na_2NO_3), methanol (CH_3OH), phenol, hydrochloric acid (HCl, 36%), potassium carbonate (K_2CO_3), *N*,*N*-dimethylformamide (DMF), dichloromethane (CH_2Cl_2), chloroform were ($CHCl_3$), tetrahydrofuran (THF) and dioxane were purchased from Sinopharm. DMF was dehydrated before use. All other reagents were commercial grade and used as received.

Synthesis of 4,4-dihydroxyazobenzene (Azo)

4-Aminophenol (10 g, 90 mmol) was dissolved in 100 mL of 1 M HCl solution, and then the mixture was cooled to 0 °C in an ice bath. Sodium nitrite (6.30 g, 90 mmol) dissolved in 150 mL of water was added drop-wise slowly at 0 °C and 200 mL pre-cooled methanol was then poured in. Then, phenol (8.55 g, 90 mmol), which was dissolved in 32.5 mL of 3 M NaOH solution, was added drop-wise slowly at 0 °C. The solution was returned to room temperature and stirred for 2 h. Methanol was removed by evaporation. The precipitation appeared after acidification with 1 M HCl and was filtered. The residue was washed with water until neutralized. The crude product was recrystallized from an ethanol/water (v/v = 1/2) mixture. An orange solid was harvested by filtering and drying. (4.9 g 25% yield) ^{1}H NMR (400 MHz, d_6-DMSO, TMS): δ (ppm) = 10.13 (s, 2H, –OH), 7.71 (m, 4H, Ar–N), 6.89 (m, 4H, Ar–O). ^{13}C NMR (400 MHz, d_6-DMSO, TMS): δ (ppm) = 116.5, 125.1, 146.0, 160.8. HRMS (ESI-MS): *m*/*z* calculated for [M ($C_{12}H_{10}N_2O_2$) + H]$^+$, 215.1; found 215.1. Mp: 204 °C.

Synthesis of Azo-C_{12}

4,4-Dihydroxyazobenzene (5.64 g, 26.40 mmol) and K_2CO_3 (36.4 g, 264 mmol) were added in 100 mL of dry DMF, and stirred for 15 min. Then 2-(2-(2-chloroethoxy)ethoxy)ethanol (13.28 g, 79 mmol) and potassium iodide (0.035 g, 0.21 mmol) were added to the reaction mixture. After refluxing for 24 h, the reaction was filtered and spun-dried. The residue was dissolved in dichloromethane, and then separated with dilute hydrochloric acid and washed with distilled water three times. The crude product was recrystallized from chloroform after the solvent was removed by evaporation. An orange product was obtained. (5.02 g 42% yield) ^{1}H NMR (400 MHz, d_6-DMSO, TMS): δ (ppm) = 7.85–7.82 (d, 4H, Ar–N), 7.14–7.11 (d, 4H, Ar–O), 4.61–4.59 (t, 2H, –*OH*), 4.20 (m, 4H, Ar–O–CH_2), 3.76 (t, 4H, –CH_2–O), 3.61–3.43 (m, 16H, CH_2CH_2–O–CH_2CH_2). ^{13}C NMR (400 MHz, d_6-DMSO, TMS): δ (ppm) = 161.3, 146.9, 124.5, 115.4, 72.8, 70.5, 70.3, 69.3, 68.1, 60.7. HRMS (ESI-MS): *m*/*z* calculated for [M ($C_{24}H_{34}N_2O_8$) + H]$^+$, 479.2; found 479.2. Mp: 120 °C.

Synthesis of Azo-mLCP

Azo-C_{12} (3.20 g 6.69 mmol) and diethyl acetamidomalonate (1.45 g 6.69 mmol) were placed in a three-necked flask equipped with a mechanical stirrer, a nitrogen inlet and a nitrogen outlet, and a distillation trap was connected to a vacuum line. The solution (10 wt% solution of $Ti(O^iPr)_4$ in ethyleneglycol dimethyl ether) as a catalyst was added into the reaction mixture. The gas inside the flask was exchanged by argon three times to remove the oxygen. The reactants were molten at 155 °C and stirred for 15 min. The inert gas was kept to flow until the bubbles disappeared for the removal of the by-product ethanol. The reaction was employed under a low vacuum for 2 h and the temperature was increased to 160 °C. Then the reaction was kept under high vacuum for 3 h until the reaction was over. The crude product was dissolved in DMF and precipitation was repeated into diethyl ether for purification (Scheme 1).

The product was dried at 90 °C in a vacuum oven for 48 h. (3.69 g 85% yield) ^{1}H NMR (400 MHz, d_6-DMSO, TMS): δ (ppm) = 8.85–8.83 (d, 1H, NH–C(O)CH_3), 7.80–7.79 (d, 4H, Ar–Ar), 7.09–7.07 (d, 4H, Ar–N–), 5.15–5.13 (d, 1H,C(O)–CH_2–C(O)), 4.23–4.16 (d, 4H, Ar–O–CH_2), 3.75–3.56 (m, 20H, CH_2CH_2–O–CH_2CH_2), 1.91 (s, 3H, NH C(O) CH_3); GPC (DMF): M_n = 15 200 g mol^{-1}, M_w/M_n = 1.51.

Characterization

^{1}H and ^{13}C NMR spectra were recorded on a Bruker AV400 NMR spectrometer using d_6-DMSO and d_8-dioxane as the solvent and TMS as the internal reference.

Wide-angle X-ray diffraction was performed using a Xenocs Xeuss 2.0 model. The X-ray source and the detector were MetalJet-D2, Excillum and Pilatus3R 1 M, Dectris, respectively.

Electron spray ionization mass spectroscopy (ESI-MS) analysis was performed on a Bruker microOTOF-QII spectrometer.

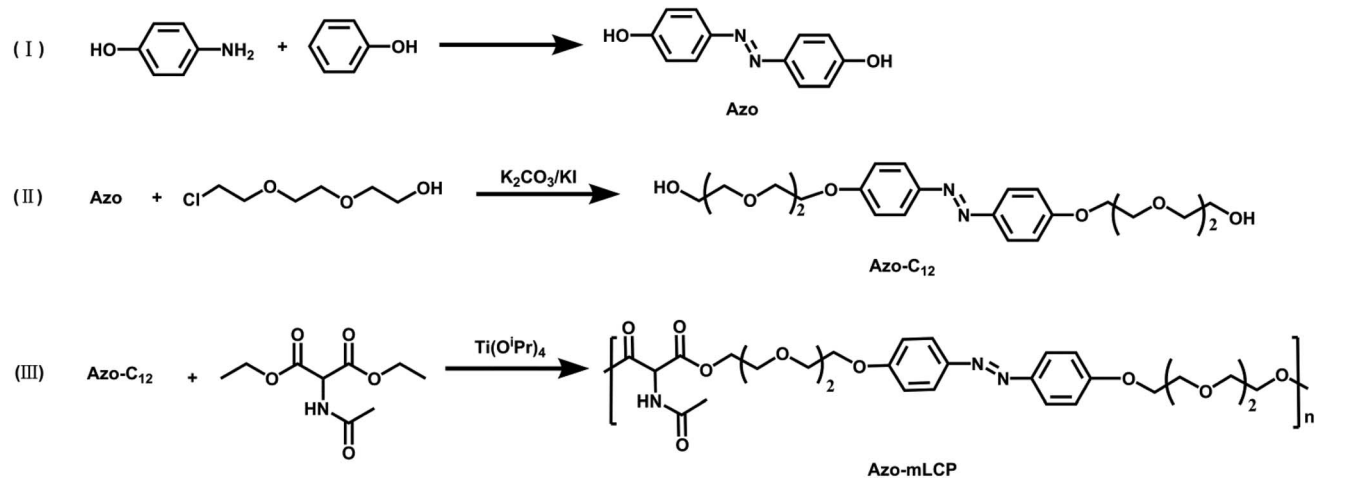

Scheme 1 Synthetic routes of Azo-mLCP.

The phase-transition temperature was measured using a DSC Q-2000 (TA Instruments, USA) at a heating rate of 10 °C min^{-1}.

Rheological properties were measured in a parallel plate with a diameter of 25 mm (PP25 and space 0.5 mm) on a rheometer MCR 302 (Anton Paar, Austria). For the pattern of oscillatory shear, we used the semiconductor temperature controller of P-PTD200. The samples were heated to 90 °C and maintained for 3 min to make completely sure they were clear and transparent. They were then cooled to 20 °C and held for 40 min to form a stable gel. Frequency sweeps were carried out at $\gamma = 0.05\%$, with the angular frequency (ω) set ranging from 0.1 to 100 rad s^{-1}.

The micromorphologies of the xerogel were characterized by SEM (Sirion 200, FEI) and AFM (Shimadzu SPM-9700).

UV-Vis absorption spectra were recorded on a diode-array spectrophotometer (Shimadzu UV-2550) at room temperature. The cell path length was 1.0 cm.

The falling ball method was used to measure the gel–sol transition temperature (T_{GS}) of the organogel at different concentrations. Steel balls (ϕ = 1 mm) were placed on the surface of the gel inside the sample vials (ϕ = 10 mm). The samples were heated until the steel ball fell to the bottom of the bottle and the temperature was T_{GS}.

The morphologies of the organogel and xerogel were observed on a polarized optical microscope (Zeiss Axio Scope P1, Germany) with a hot stage (Linkam THMS 600).

GPC analysis was performed on a Waters 1515-2414 apparatus equipped with a refractive index detector, using monodispersed PMMA standards to get a calibration curve. The elution solvent was DMF at a flow rate of 1 mL min^{-1} at 40 °C.

Results and discussion

Gelation ability of Azo-mLCP

In this study, we synthesized an azobenzene-containing main-chain LCP (Azo-mLCP) as a gelator for organic solvents. As listed in Table 1, the gelation ability of Azo-mLCP in common solvents has been examined. Azo-mLCP can form a gel in dioxane and THF, but dissolves in chloroform and DMF. In terms of the Kamlet–Taft parameters, hydrogen-bond-mediated gelation is primarily dependent on α (the ability of a solvent to donate a proton), and has a secondary dependence on β (the ability of a solvent to accept a proton), but exhibits a slight dependence on π^* (the index of solvent dipolarity).[21] In Table S1 (ESI†), the α value of chloroform, as well as the π^* and β values of DMF are greater than the corresponding value for THF and dioxane. Therefore, Azo-mLCP can dissolve in chloroform and DMF instead of forming a gel. Besides, dioxane has a lower β value than THF, so the corresponding gel would display a lower minimum gelation concentration (MGC). As expected, the MGC of Azo-mLCP in dioxane (6.5 wt%) was indeed lower

Table 1 Gelation ability and MGC of Azo-mLCP

Solvent	Gelation ability[a]	MGC (wt%)	Solvent	Gelation ability	MGC (wt%)
Dioxane	G	6.5	THF	G	9.5
Chloroform	S	—	DMF	S	—
Ethyl acetate	P	—	Acetonitrile	P	—
Acetone	P	—	Methanol	P	—
Methylbenzene	P	—	Water	P	—

[a] G = gel; P = precipitate; S = solution.

than that in THF (9.5 wt%). Therefore, we focused on the gel formed in dioxane for the following investigations.

As shown in Fig. 1, the gels have a reversible responsiveness to temperature. The gel–sol transition temperature (T_{GS}) was tested at 44 °C by the falling ball method with 8 wt% Azo-mLCP in dioxane. When the temperature was greater than T_{GS}, a reddish-brown clear solution was obtained. A stable gel could be formed again after cooling to room temperature. The ^{1}H NMR spectra of Azo-mLCP in d_8-dioxane at different concentrations were studied to determine the driving force of the gel. Fig. 2a and S1 (ESI†) show that the double peaks of azobenzene protons and amide proton could be observed below 4.50 mM, but gradually merged into a broad single peak with increasing concentration. Meanwhile, the intensities of azobenzene protons and amide proton decreased with the increase in concentration. It is obvious that the protons of Azo-mLCP were not equivalent in the gel state.[22] The results suggest that the Azo-mLCP chains were in the isolated state below 2.25 mM, which is consistent with the MGC value of 6.5 wt%, and then started to self-assemble *via* hydrogen bonding above 2.25 mM. In addition, the FTIR spectra in Fig. 2b show that the NH and CO stretching modes were located at 3257 and 1674 cm^{-1} in the pure polymer, respectively. For the gel, the NH peak became wider while the CO peak was shifted to the lower wavenumber of 1666 cm^{-1}. That is, both the ^{1}H NMR and FTIR spectra indicated that the polymeric gelator could self-assemble to form an organogel in dioxane *via* hydrogen bonds between the pendent amide groups.

Rheological properties of the Azo-mLCP organogel

The rheological results of the organogels with different concentrations at 5.5–10.5 wt% are shown in Fig. 3. The storage modulus (G') and the loss modulus (G'') were independent of the strain in the linear viscoelastic region (LVR), which indicated that the organogels were stable under such a strain range. Fig. 3a shows that G' was higher than G'' at low strains, which is the characteristic for a typical solid-like gel. The network collapsed when the strain exceeded a critical value. Then, the frequency sweep was tested within LVR. As shown in Fig. 3b and c, the mixture was liquid when the Azo-mLCP concentration was below the MGC, *i.e.* 5.5 wt%. The gelators started to assemble into a network with the increase in concentration. Meanwhile, G' increased rapidly from 10^3 Pa to 10^5 Pa. When the concentration was higher than 7.5 wt%, the gel had a self-supporting ability with $G' > 10^4$ Pa.[23] The good mechanical property of the organogel was probably related to the microscopic ordered arrangement of the LCP gelator.

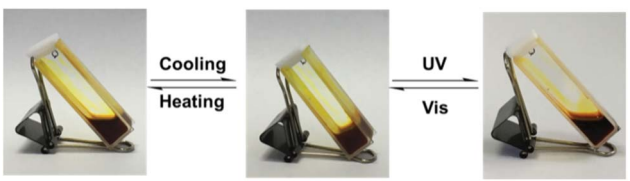

Fig. 1 Photographs of the dual stimuli-responsive behaviours of the organogel with 8 wt% Azo-mLCP in dioxane.

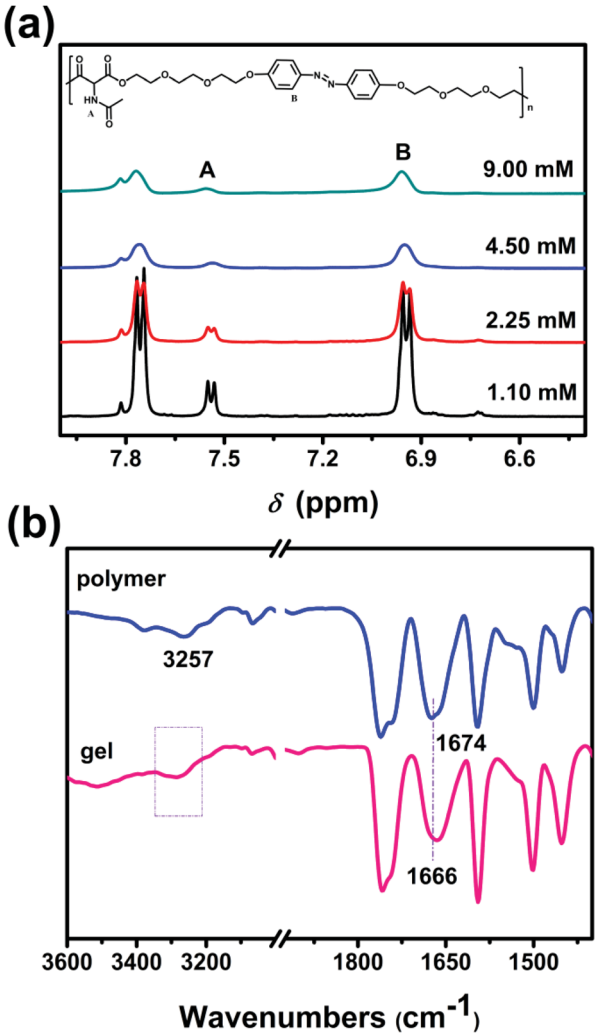

Fig. 2 (a) Partially zoomed ^{1}H NMR spectra of Azo-mLCP in d_8-dioxane at different concentrations. The inset of (a) shows the molecular structure of Azo-mLCP. (b) FTIR spectra of the polymer and gel in dioxane.

Photoresponsive behaviours of the Azo-mLCP in solution and in the organogel

Due to the azobenzene groups in the backbone of Azo-mLCP, the UV-Vis absorption spectra were used to confirm their *trans–cis* isomerization in solution as shown in Fig. 4. The π–π* absorption peak of the *trans*-isomer at 358 nm decreased gradually and the n–π* absorption peak of the *cis*-isomer at 450 nm increased slightly upon UV light irradiation. The photostationary state was reached after 78 s under UV light irradiation. Reversibly, visible light irradiation resulted in the recovery of the *trans*-azo. Meanwhile, the maximum absorption wavelength was shifted from 358 to 312 nm under UV light irradiation and went back upon visible light irradiation, implying a π–π stacking between the *trans*-azo moieties. Two isosbestic points could be observed at 318 and 426 nm, which confirmed that only the *cis* and *trans* absorbing species were present in solution.[24] The first-order kinetic equation about the *trans*-to-*cis* isomerization of azobenzene was calculated as follows:[25]

$$\ln\frac{A_\infty - A_t}{A_\infty - A_0} = -K_{tc}t$$

where A_0, A_t and A_∞ are the absorbance values before irradiation, after irradiation for t and at the photo-stationary state, respectively. K_{tc} is the constant of photo-isomerization. According to the linear fitting, the K_{tc} for Azo-mLCP in dioxane could be calculated as 0.035 s^{-1} when the intensity of UV light was only 0.28 mW cm^{-2}. There are rarely reports about such a low intensity except that the PAA-Azo can reach the photo-stationary state after 90 s under UV light irradiation at 0.45 mW cm^{-2}.[9] In fact, the obtained K_{tc} linearly depends on the light intensity at a specific irradiation wavelength.[24] When the intensity of UV light irradiation was only about one-tenth of the most intensities listed in Table S2 (ESI†), Azo-mLCP could reach a photo-stationary state with a smaller t_∞.[9,26–32] Compared with

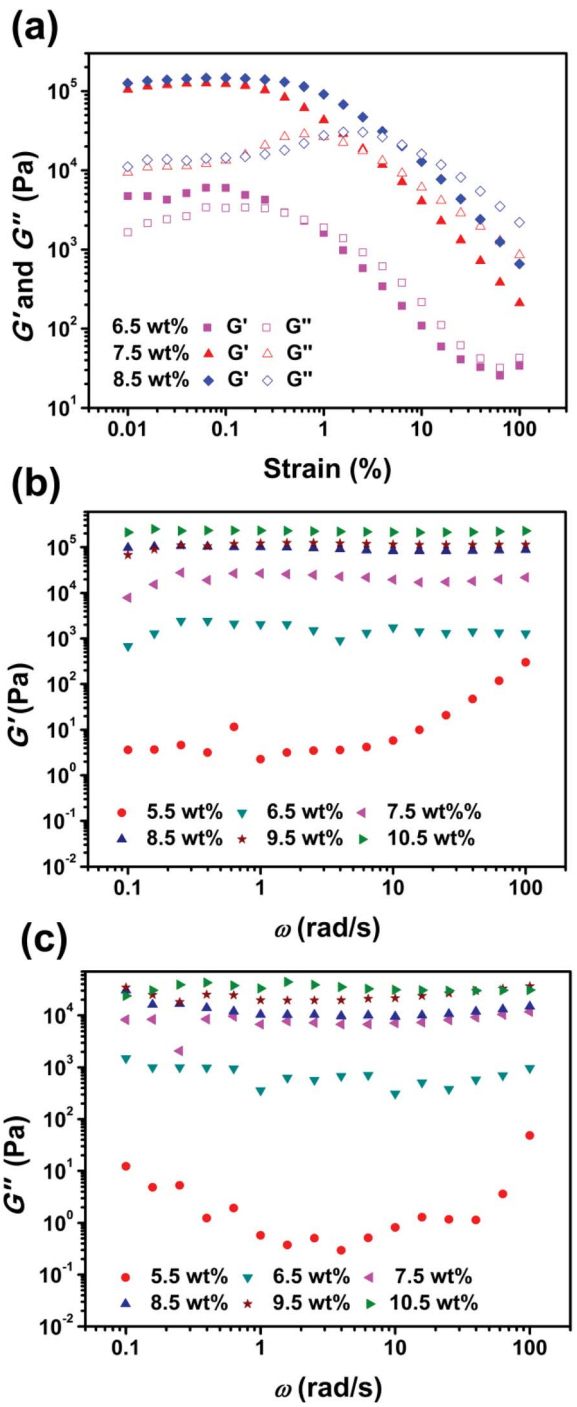

Fig. 3 (a) Strain and (b and c) frequency sweeps for the Azo-mLCP organogels at different concentrations.

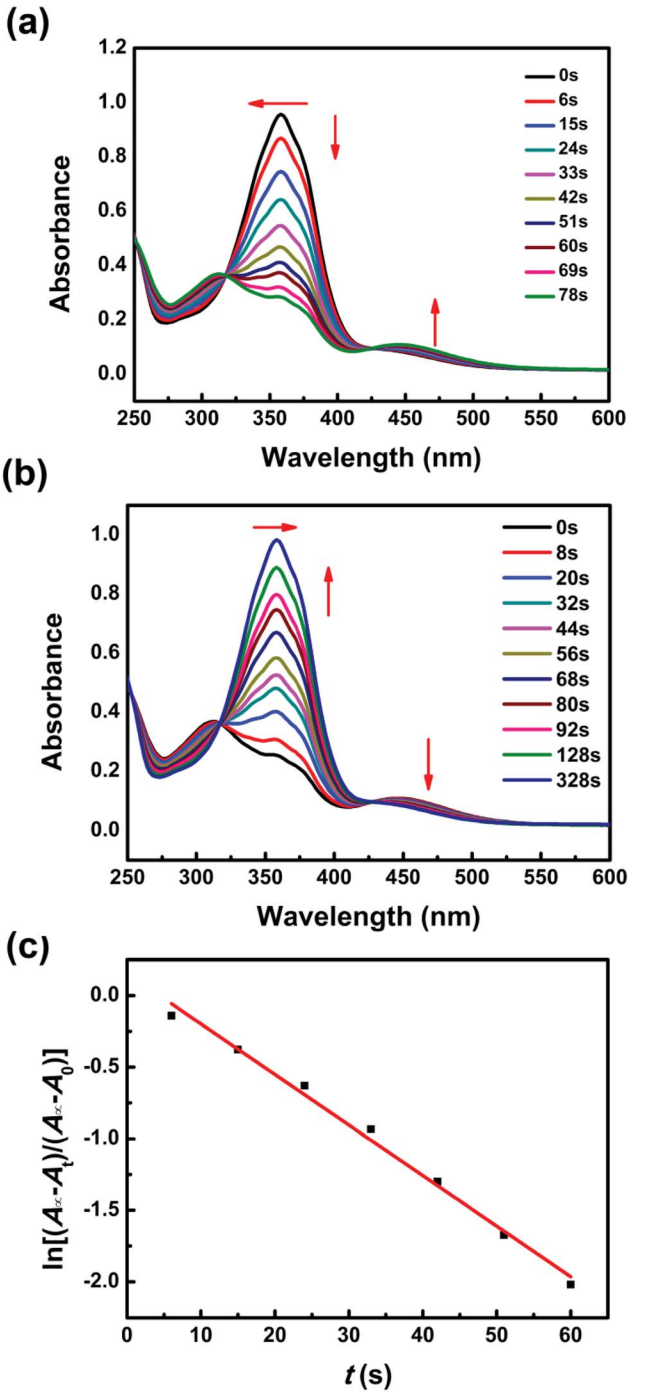

Fig. 4 UV-Vis absorption spectra of Azo-mLCP in dioxane (1×10^{-4} mol L^{-1}) (a) irradiated by UV light (365 nm, 0.28 mW cm^{-2}) and then (b) irradiated by visible light (550 nm, 2.10 mW cm^{-2}). (c) Kinetic curve of the *trans*-to-*cis* isomerization of Azo-mLCP in dioxane.

most azobenzene-containing polymers and small molecules, our Azo-mLCP displayed a larger constant of photo-isomerization under a lower UV light intensity. This was mainly attributed to the coupling effect between the photo-isomerization reaction and the conformation of the liquid crystal polymer chain being stronger when the photo-responsive group is located on the main chain.[15]

As shown in Fig. 5a, the ^{1}H NMR spectra of Azo-mLCP before and after UV irradiation were measured to explore the ratio of *trans*- and *cis*-isomers of azobenzene at the photo-stationary state. Before irradiation, the two double proton peaks of benzene appeared at 6.96 and 7.77 ppm, respectively. After irradiation for 10 min to ensure a photo-stationary state, the two double peaks perfectly merged into a quadruple peak at a lower chemical shift of 6.73 ppm. In other words, almost all the *trans*-azobenzene was isomerized to *cis*-azobenzene in solution upon UV irradiation.[33] Azo-mLCP could not only undergo quick photo-isomerization under such a low UV light intensity, but also converted completely from *trans*-azo to *cis*-azo. To the best of our knowledge, this is the first example for azobenzene-containing polymers. In addition, the exact proportion of *cis*-isomers to trigger a gel-to-sol transition is important for understanding the construction mechanism of photo-responsive gels. As shown in Fig. 5b, after UV irradiation, the peak at 6.73 ppm for *cis*-azobenzene in the sol increased dramatically, while the peaks at 7.77 ppm and 6.96 ppm for *trans*-isomer decreased simultaneously. Therefore, the percentage of *cis*-isomers during the *trans*-to-*cis* transformation could be calculated as 48% by comparing their integral. This is rational because our organogel was robust. Finally, upon visible light irradiation, the peaks for *trans*-azobenzene protons returned to the original state, while the peak for *cis*-isomer disappeared. The incomplete *trans*-to-*cis* conversion strategy could efficiently trigger the gel-to-sol process of the organogel with the external stimulus.[34] However, due to the hydrogen bond and π–π interactions between the polymer chains in the organogel, the movement space of Azo-mLCP was confined. Thus, the isomerization process of the macromolecular backbone was depressed, which resulted in the UV light intensity for the photo-isomerization for the polymeric gelator in the organogel being higher than in solution.

In order to further investigate the changes in the morphology of the gels before and after UV irradiation, FE-SEM and AFM

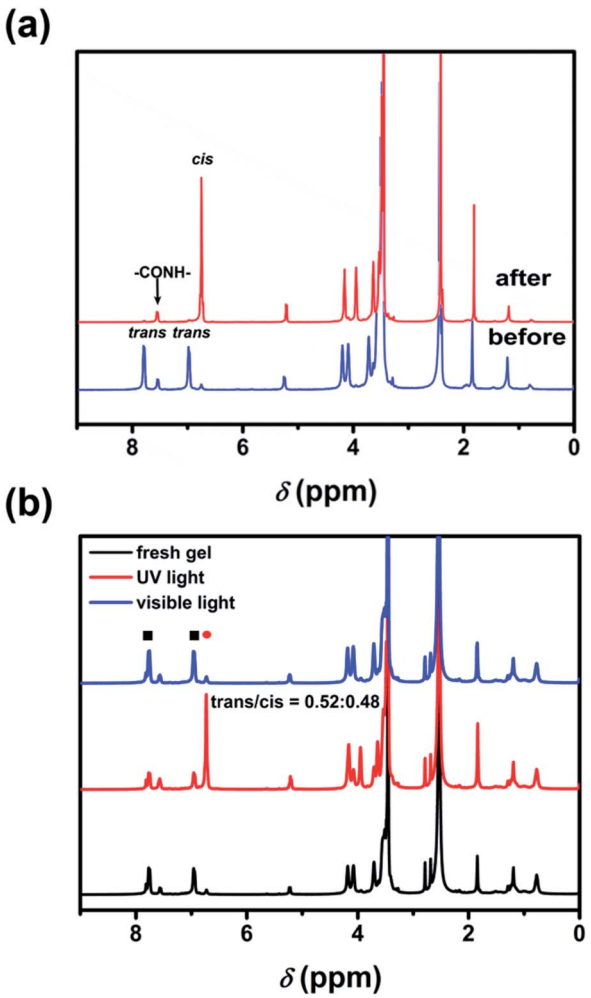

Fig. 5 (a) ^{1}H NMR spectra of Azo-mLCP in d_8-dioxane before (bottom) and after UV irradiation (365 nm, 0.28 mW cm^{-2}) for 10 min (top). (b) ^{1}H NMR spectra compositions of the gel based on Azo-mLCP (bottom), after UV light irradiation (middle), and subsequent irradiation under visible light (top). The black squares and the red circle represent the proton peaks of *trans*- and *cis*-isomer of azobenzene, respectively. The gel is prepared in d_8-dioxane at a concentration of 7.5 wt%.

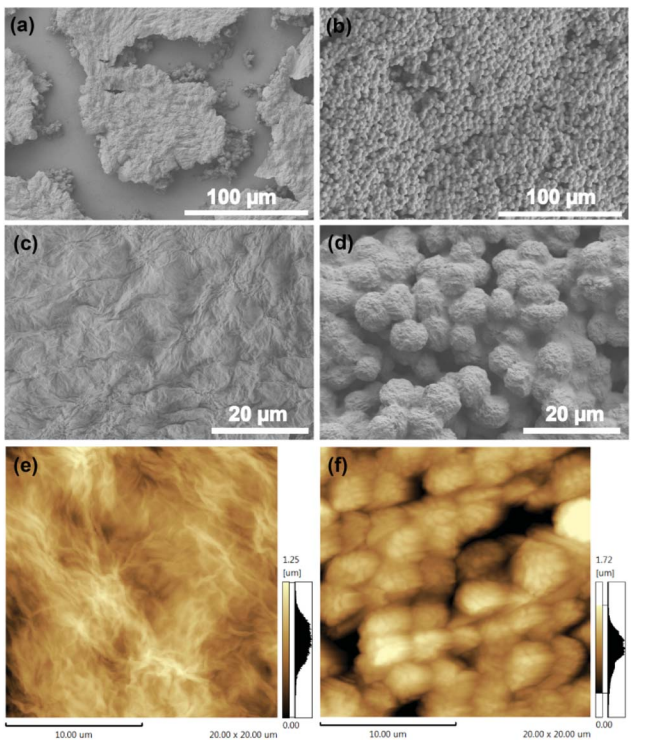

Fig. 6 (a and c) FE-SEM and (e) AFM images of Azo-mLCP xerogels formed in dioxane without UV irradiation, (b and d) FE-SEM and (f) AFM images of xerogels with UV irradiation.

images of the Azo-mLCP xerogels were obtained. The organogels with 10 wt% Azo-mLCP were placed in a vacuum oven at 40 °C for 3 days to remove the solvent completely. For the gels before UV irradiation, Fig. 6a and c show a wrinkled dry-muddy sheet in a micrometer scale at the top and irregular aggregates at the bottom.[35] This wrinkled dry-muddy sheet has also been observed in the gels made of peptides bearing an azobenzene moiety.[36] In addition, the same morphology was observed in the AFM image as shown as Fig. 6e, so the top wrinkled dry-muddy sheet should not be ascribed to the collapse under electron beam. It is interesting that the morphology of the organogel varied to coffee-bean-like particles with a diameter of about 3 μm after UV irradiation in Fig. 6b and d, which was consistent with the AFM observation in Fig. 6f. These results confirmed that the UV light could change the azobenzene configuration and polymer backbone conformation, leading to the destruction of the gel structure.

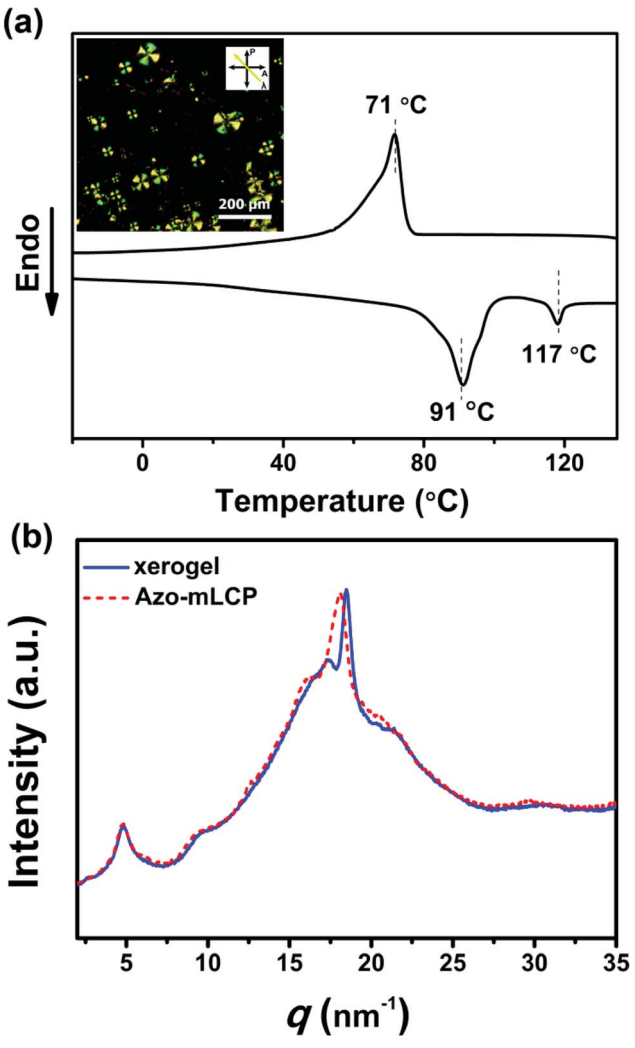

Fig. 7 (a) DSC curves of xerogel tested on the first cooling and second heating scans in N_2 at a heating rate of 10 °C min^{-1}. The inset of (a) shows a POM photograph of the xerogel captured at 69 °C. P, polarizer; A, analyzer; λ, phase retarder. (b) 1D WAXD patterns of xerogel and Azo-mLCP.

The liquid crystalline behaviour of the Azo-mLCP organogel

The liquid crystalline behaviour of the xerogel was investigated by DSC and POM. The texture of Azo-mLCP during the cooling process was observed by POM. It showed a typical focal-conical texture, which usually corresponds to the smectic phase.[37] In Fig. 7a, the DSC curves of the xerogel showed an endothermic peak at 91 °C, which could be assigned to the phase transition from smectic to isotropic, while the exothermal peak at 71 °C was attributed to the isotropic-to-smectic phase transition. In addition, the wide-angle X-ray diffraction (WAXD) of the xerogel displayed a broad peak at 17 nm^{-1}, corresponding to the interaction of the ether chain and a peak at 21 nm^{-1}, corresponding to the π–π stacking azobenzene mesogen in Fig. 7b. At room temperature, three peaks could be observed at 4.84 nm^{-1} (1.30 nm), 9.30 nm^{-1} (0.68 nm) and 18.45 nm^{-1} (0.34 nm), respectively. The q ratio of 1 : 2 : 4 means that the xerogel still displayed a smectic phase in the gel state. Besides, the q value at 18.45 nm^{-1} for the xerogel was higher than the as-prepared Azo-mLCP at 18.10 nm^{-1}, which suggests that the distance between the mesogens became shorter during the gelation process.[38] The birefringence of the Azo-mLCP organogel disappeared while the isotropic sol appeared after UV light irradiation, as seen in Fig. S2 (ESI†), which indicates the liquid crystalline property of Azo-mLCP could be destroyed during the gel-to-sol transition.

As shown in Scheme 2, we drew a model for describing the microstructure changes for the reversible gel-to-sol processes of the Azo-mLCP organogel upon UV and visible light irradiation. Smectic Azo-mLCP self-assembled to fibrils through hydrogen bonds and weak π–π interactions. These fibrils then further formed a gel network to entrap solvents. After a part of the azobenzene groups isomerized from *trans* to *cis* configurations under UV irradiation, the liquid crystallinity of the gelator could be destroyed. Meanwhile, the backbone conformation and the ordered stacking microstructures could be changed so that the solvents could not continue to be anchored. It is interesting that the network and the organogel could be rebuilt after visible light irradiation.

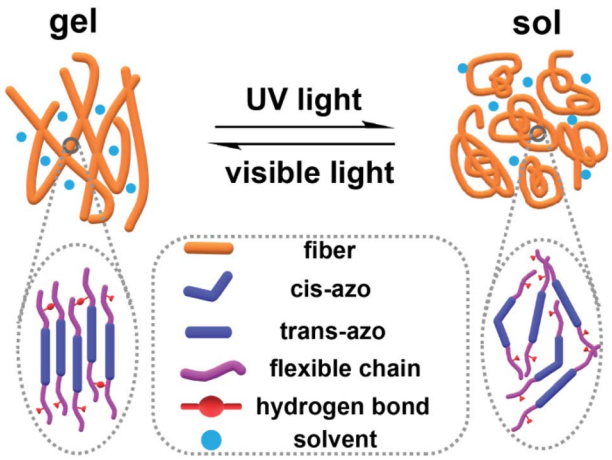

Scheme 2 Microscopic schematic illustration for the reversible gel–sol process of the Azo-mLCP organogel under UV light and visible light irradiation.

Conclusions

In summary, we obtained a photo-responsive liquid crystalline polymer organogel bearing the azobenzene group in the polymer main chain. The robust organogel could be constructed by hydrogen bonds of the pendent amide group and π–π interactions of azobenzene. The Azo-mLCP gelator underwent fast *trans*-to-*cis* transformation in solution under UV irradiation with an ultra-low intensity. In addition, the efficiently reversible gel-to-sol transition could be triggered when about half *trans*-azobenzene transformed to *cis*-azobenzene. The good mechanical property of the organogel was closely related to the introduction of the main-chain LCP gelator, while the efficient photomechanical effect was attributed to the incomplete *trans*-to-*cis* conversion strategy. This work provides some inspiration for the fabrication of smart photo-responsive materials and broadens the applications ranging from actuators to electro-optical devices.

Conflicts of interest

There are no conflicts to declare.

Acknowledgements

We acknowledge the financial support of the National Natural Science Foundation of China (51773070, 51973072, and 51433002). We greatly appreciate Dr Shitao Fu for the measurements and analyses of ^{1}H and ^{13}C NMR spectra. We also thank the HUST Analytical and Testing Center for AFM measurement.

Notes and references

1 X. Yan, F. Wang, B. Zheng and F. Huang, *Chem. Soc. Rev.*, 2012, **41**, 6042–6065.
2 C. D. Jones and J. W. Steed, *Chem. Soc. Rev.*, 2016, **45**, 6546–6596.
3 O. Bertrand and J.-F. Gohy, *Polym. Chem.*, 2017, **8**, 52–73.
4 X. Wang, Y. Yang, Z. Yang, X. Zhou, Y. Liao, C. Lv, F. –C. Chang and X. Xie, *J. Therm. Anal. Calorim.*, 2010, **102**, 739–744.
5 Q. Chen, D. Zhang, G. Zhang, X. Yang, Y. Feng, Q. Fan and D. Zhu, *Adv. Funct. Mater.*, 2010, **20**, 3244–3251.
6 H. Tian and S. Yang, *Chem. Soc. Rev.*, 2004, **33**, 85–97.
7 M. Alemani, M. V. Peters, S. Hecht, K.-H. Rieder, F. Moresco and L. Grill, *J. Am. Chem. Soc.*, 2006, **128**, 14446–14447.
8 G. S. Kumar and D. C. Neckers, *Chem. Rev.*, 1989, **89**, 1915–1925.
9 Y. Xiong, Z. Chen, H. Wang, L. M. Ackermann, M. Klapper, H. J. Butt and S. Wu, *Chem. Commun.*, 2016, **52**, 14157–14160.
10 K. Peng, I. Tomatsu and A. Kros, *Chem. Commun.*, 2010, **46**, 4094–4096.
11 H.-Z. Wang and H.-F. Chow, *Chem. Commun.*, 2018, **54**, 8391–8394.
12 L. Fang, H. Zhang, Z. Li, Y. Zhang, Y. Zhang and H. Zhang, *Macromolecules*, 2013, **46**, 7650–7660.
13 A. S. Angeloni, D. Caretti, C. Carlini, E. Chiellini, G. Galli, A. Altomare, R. Solaro and M. Laus, *Liq. Cryst.*, 1989, **4**, 513–527.
14 T. Yoshino, M. Kondo, J. i. Mamiya, M. Kinoshita, Y. Yu and T. Ikeda, *Adv. Mater.*, 2010, **22**, 1361–1363.
15 P. M. Hogan, A. R. Tajbakhsh and E. M. Terentjev, *Phys. Rev. E*, 2002, **65**, 041720.
16 P. E. Cladis, Liquid crystalline elastomers as artificial muscles, in *Dynamic Control System Conference Proceedings*, Canada, 2001.
17 T. J. White and D. J. Broer, *Nat. Mater.*, 2015, **14**, 1087–1098.
18 M. Petr and P. T. Hammond, *Macromolecules*, 2011, **44**, 8880–8885.
19 X. Wang, Y. Yang, Y. Liao, Z. Yang, M. Jiang and X. Xie, *Eur. Polym. J.*, 2012, **48**, 41–48.
20 X. Wang, Z. Li, Y. Yang, X. Gong, Y. Liao and X. Xie, *Langmuir*, 2015, **31**, 5456–5463.
21 W. Edwards, C. A. Lagadec and D. K. Smith, *Soft Matter*, 2011, **7**, 110–117.
22 C. Po, Z. Ke, A. Y. Tam, H. F. Chow and V. W. Yam, *Chem. –Eur. J.*, 2013, **19**, 15735–15744.
23 S. Bi, H. Peng, S. Long, M. Ni, Y. Liao, Y. Yang, Z. Xue and X. Xie, *Soft Matter*, 2013, **9**, 8855–8858.
24 D. Acierno, E. Amendola, V. Bugatti, S. Concilio, L. Giorgini, P. Iannelli and S. P. Piotto, *Macromolecules*, 2004, **37**, 6418–6423.
25 O. Tsutsumi, T. Shiono, T. Ikeda and G. Galli, *J. Phys. Chem. B*, 1997, **101**, 1332–1337.
26 W. Cheng, D. Zhao, Y. Qiu, H. Hu, H. Wang, Q. Wang, Y. Liao, H. Peng and X. Xie, *Soft Matter*, 2018, **14**, 5213–5221.
27 R. Yin, W. Xu, M. Kondo, C.-C. Yen, J.-I. Mamiya, T. Ikeda and Y. Yu, *J. Mater. Chem.*, 2009, **19**, 3141–3143.
28 H. Hu, Y. Qiu, J. Wang, D. Zhao, H. Wang, Q. Wang, Y. Liao, H. Peng and X. Xie, *Macromol. Rapid Commun.*, 2019, **40**, 1800629.
29 D. Zhao, Y. Qiu, W. Cheng, S. Bi, H. Wang, Q. Wang, Y. Liao, H. Peng and X. Xie, *Langmuir*, 2018, **34**, 700–708.
30 M. R. Han and M. Hara, *New J. Chem.*, 2006, **30**, 223–227.
31 Z. Yan, X. Ji, W. Wu, J. Wei and Y. Yu, *Macromol. Rapid Commun.*, 2012, **33**, 1362–1367.
32 Z. Feng, L. Lin, Z. Yan and Y. Yu, *Macromol. Rapid Commun.*, 2010, **31**, 640–644.
33 X. Yu, H. Chen, X. Shi, P.-A. Albouy, J. Guo, J. Hu and M.-H. Li, *Mater. Chem. Front.*, 2018, **2**, 2245–2253.
34 Z. Yu and S. Hecht, *Angew. Chem., Int. Ed.*, 2011, **50**, 1640–1643.
35 T. Jiao, Q. Huang, Q. Zhang, D. Xiao, J. Zhou and F. Gao, *Nanoscale Res. Lett.*, 2013, **8**, 278.
36 P. Fatas, J. Bachl, S. Oehm, A. I. Jimenez, C. Cativiela and D. Diaz Diaz, *Chem. –Eur. J.*, 2013, **19**, 8861–8874.
37 I. Dierking, *Textures of Liquid Crystals*, WILEY-VCH Verlag GmbH, Weinheim, 2003.
38 J. Wang, X. Hao, H. Yan, Q. Jiang, H. Peng, B. Xiong, Y. Liao and X. Xie, *Polymer*, 2020, 122148.